Title

Mechanical Properties of Solidifying Assemblies of Nanoparticle Surfactants at the Oil—Water Interface

Journal

Langmuir, 35(41)

ISSN

0743-7463

Authors

Toor, Anju

Forth, Joe

de Araujo, Simone Bochner

et al.

Publication Date

2019-10-15

DOI

10.1021/acs.langmuir.9b01575

Peer reviewed

Mechanical Properties of Solidifying Assemblies of Nanoparticle Surfactants at the Oil−Water Interface

Anju Toor,[†,‡] Joe Forth,[‡] Simone Bochner de Araujo,[§] Maria Consiglia Merola,[§] Yufeng Jiang,[‡,∥] Xubo Liu,[‡,⊥] Yu Chai,[‡,∥,#] Honghao Hou,[‡] Paul D. Ashby,[‡,#] Gerald G. Fuller,[§] and Thomas P. Russell*[,‡,⊥,¶,▽]

[†]Department of Mechanical Engineering, University of California, 6141 Etcheverry Hall, Berkeley, California 94720, United States

[‡]Materials Sciences Division, Lawrence Berkeley National Laboratory, 1 Cyclotron Road, Berkeley, California 94720, United States

[§]Department of Chemical Engineering, Stanford University, 443 Via Ortega, Stanford, California 94305, United States

[∥]Department of Applied Science and Technology, University of California, Berkeley, California 94720, United States

[⊥]Beijing Advanced Innovation Center for Soft Matter Science and Engineering, Beijing University of Chemical Technology, Beijing 100029, China

[#]The Molecular Foundry, Lawrence Berkeley National Laboratory, 1 Cyclotron Road, Berkeley, California 94720, United States

[¶]Polymer Science and Engineering Department, University of Massachusetts, 120 Governors Drive, Conte Center for Polymer Research, Amherst, Massachusetts 01003, United States

[▽]Advanced Institute for Materials Research (AIMR), Tohoku University, 2-1-1 Katahira, Aoba, Sendai 980-8577, Japan

ABSTRACT: The effect of polymer surfactant structure and concen- tration on the self-assembly, mechanical properties, and solidification of nanoparticle surfactants (NPSs) at the oil−water interface was studied.

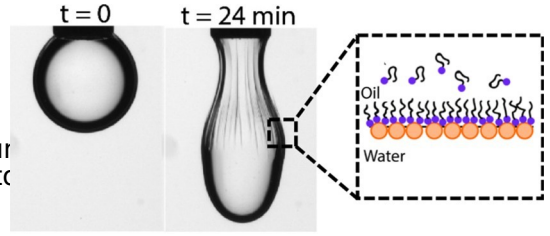

The surface tension of the oil−water interface was found strongly on the choice of the polymer surfactant used to NPSs, with polymer surfactants bearing multiple polar groups being the most effective at reducing interfacial tension and driving the NPS assembly. By contrast, only small variations in the shear modulus of the system were observed, suggesting that it is determined largely by particle density. In the presence of polymer surfactants bearing multiple functional groups, NPS assemblies on pendant drop surfaces were observed to spontaneously solidify above a critical polymer surfactant concentration. Interfacial solidification accelerated rapidly as polymer surfactant concentration was increased. On long timescales after solidification, pendant drop interfaces were observed to spontaneously wrinkle at sufficiently low surface tensions (approximately 5 mN m^{-1}). Interfacial shear rheology of the NPS assemblies was elastic-dominated, with the shear modulus ranging from 0.1 to 1 N m^{-1}, comparable to values obtained for nanoparticle monolayers elsewhere. Our work paves the way for the development of designer, multicomponent oil−water interfaces with well-defined mechanical, structural, and functional properties.

INTRODUCTION

The assembly of nanoparticles (NPs) at the liquid−liquid interface provides a versatile platform to produce dimension- ally confined materials that possess novel mechanical, and functional properties.[1−3] NP assemblies can also be used to lock liquids into complex nonequilibrium shapes by interfacial jamming of NPs, with the mechanical properties of the assembly determining the mechanical properties of the stabilized structure.[4−6] Nanoparticle surfactants (NPSs), which consist of functionalized NPs dispersed in one liquid phase and polymer surfactants dispersed

in a second, immiscible liquid phase, are a particularly powerful platform for assembling highly controlled nanomaterials at the oil− water interface.[7−9] The particles and polymers in these systems are confined within immiscible bulk liquid phases and interact at the liquid−liquid interface to form a layer of NPSs. This synergistic mechanism for engineering NP adsorption at the oil−water interface bypasses the need for painstaking tuning of the surface chemistry of NPs and solvent properties.[4,10] NPS assemblies are also remarkably versatile. Successful assembly of NPSs at the oil−water interface requires only that the polymers and NPs have complementary functional groups (e.g., ion-pairing); gold NPs, graphene oxide nanosheets, polyoxometalates, cellulose nanocrystals, and carbon nano- tubes have all been used to shape liquids into complex structures.[11−15]

As NPS concentration at the oil−water interface increases, NPSs undergo a transition from a dynamic, that is, liquid-like

state, to a kinetically arrested, solid-like, load-bearing state that can be used to structure liquids into complex shapes.[16] We refer to this transition here as 'interfacial solidification'. In this work, we study the assembly of NPSs at the oil−water interface during and after interfacial solidification and investigate how the structure and concentration of the polymer surfactant affects the shear moduli of NPS assemblies and surface tension, γ, of the oil−water interface. The surface stress tensor, τ_{ij}, in our solidifying interfaces has two distinct contributions[17−20]

$$\tau_{ij} = \gamma\delta_{ij} + \Gamma_{ij} \quad (1)$$

"$\gamma\delta_{ij}$" in eq 1 describes the free-energy cost per unit area associated with the existence of the oil−water interface and decreases as material adsorbs to the oil−water interface. In liquid−liquid interfaces that are either clean or contain reversibly adsorbed molecules, this is equivalent to the liquid−fluid surface tension, γ. Γ_{ij} describes anisotropic contributions to the surface stress derived from the material properties of the adsorbed layer. As the interface solidifies, this second term grows rapidly, characterized by an increase in the shear modulus of the interface. The shear moduli of NP and NPS monolayers measured elsewhere in the literature typically range from 0.1 to 1 N m^{-1} and exhibit power-law growth above an areal NP density, $\phi_a \approx 0.4$.[21−23]

The materials used here were chosen because of their relevance to the emerging field of printed and molded liquids; all three polymer surfactants have been successfully used in printed liquid applications.[5] Engineering the timescale of interfacial solidification in these systems is critical for the controlled arrest of hydrodynamic instabilities in interfacially jammed structured liquids.[11,14,24,25] Controlling the mechan- ical properties of such interfaces is critical in providing stability to the structures against Ostwald ripening and maximizing the flow-through rates for applications in chemical synthesis.[5,26−28]

Here, we show how both the shear moduli of the NPS assemblies and surface tension of the oil−water interface can be controlled simply by varying the structure and concen- tration of the polymer surfactants that are used to assemble the NPS. We used pendant drop tensiometry to investigate how the two components affect the surface tension of the system, and used image analysis methods to extract the timescale on which the interfacial assembly solidifies. We found that increasing the polymer surfactant concentration resulted in a more rapid assembly of the NPS and accelerated interfacial solidification. The interfacial shear rheology of the NPS assemblies was predominately elastic dominated. The plateau values of the shear moduli on long timescales all lay in the range 0.1−1 N m^{-1}, suggesting that, for the close-packed interfaces studied here, the shear modulus is largely determined by particle density. Remarkably, at extremely low surface tensions ($\gamma \approx 5$ mN m^{-1}), the oil−water interface was observed to spontaneously wrinkle, showing how shape evolution of interfacially structured liquids is driven by both the mechanical properties of the adsorbed layer and the surface energy of the oil−water interface.

MATERIALS AND METHODS

Sample Preparation. Silicone oil (kinematic viscosity 5 cSt, ρ = 912 kg m^{-3}) was purchased from Sigma-Aldrich and used as received. Carboxylic acid-functionalized silica NPs [diameter ≈ 14 nm, measured by dynamic light scattering (DLS)] were obtained from Microspheres-Nanospheres and used as received. 2-(*N*-Morpholino)-ethanesulfonic acid sodium salt (NaMES) was obtained from Sigma-Aldrich. Dilute dispersions of NPs were found to undergo a change in their pH on a timescale of ≈1 h after dilution, leading to poor reproducibility of the results. As such, 1 mg mL^{-1} NP dispersions were prepared in a 5 mM buffer solution of NaMES, which was shown using DLS not to cause aggregation of the NPs. The pH of the NP dispersions was adjusted to 6.4 using 1 M HCl. The surface tension of the resulting 1 mg mL^{-1} 14 nm Si particles in 5 mM MES buffer against silicone oil was measured to be γ = 35 mN m^{-1}, comparable to that of a clean water−silicone oil interface, with disparities attributed to small concentrations of surface-active impurities in both oil and the NP dispersion. Monoaminopropyl-terminated polydimethylsiloxane (PDMS−NH_2, $M_w \approx 1750$ g mol^{-1}, determined by ^{1}NMR, consistent with Xing et al.) was purchased from Gelest Inc. and used as received.[29] Bis(3-aminopropyl) terminated poly(dimethylsiloxane) ('H_2N−PDMS−NH_2', M_n = 2500 g mol^{-1}), and poly- [dimethylsiloxane-*co*-(3-aminopropyl)methylsiloxane] random co- polymer ('RCP', $M_w \approx 11\,000$ g mol^{-1}, estimated using the relation for linear siloxane polymers in ref 30), were purchased from Sigma-Aldrich and used as received. The ligand dispersions were prepared by mixing the desired amounts of amine-functionalized polymers in the silicone oil and agitating the mixture by shaking.

Pendant Drop Tensiometry. A pendant drop tensiometer (Kruss DSA30S) was used to probe the interfacial tension of the oil−water interface at which NPSs were assembling. The surface tension of the pendant drop was measured using the software provided by the equipment manufacturer. The timescale of solid- ification of the interface was defined as the time at which the mean curvature of the pendant drop was no longer a linear function of the distance from the apex of the droplet. Droplet mean curvature, $H = \frac{1}{R_1} + \frac{1}{R_2}$, was extracted from the droplets using the MATLAB scripts of Nagel [19] In order to calculate nonlinearity

curvature, the spatial derivative of the mean curvature, $H' = dH/dz$, was calculated numerically. Limitations due to camera resolution, alignment, and detector noise, and residual anisotropic stresses due to inhomogeneous wetting of the capillary, from which the needle was suspended, required an empirical noise floor in c_v to be determined for a system that exhibited only isotropic surface stresses. Calibration with a particle-free system yielded typical values for the coefficient of variation and its standard deviation, c'_v and σ'_{cv}, respectively. The solidification time of the interface was taken as the point at which the measured c_v increased monotonically past $c'_v + 3\sigma'_{cv}$ (Figures S3−S5).

Interfacial Shear Rheology. The viscoelastic properties of the NPS assemblies formed at the oil−water interface were measured using a stress-controlled discovery hybrid rheometer (DHR-3) from TA Instruments (USA) equipped with a Du Nouy ring and the double-walled Couette flow-cell geometry. The latter is made of a glass external cylinder and a Teflon internal cylinder. For H_2N−PDMS−NH_2 and RCP, the rheological study was conducted using the following protocol: (1) time sweep for 3 h at a frequency $\omega = 3.14$ rad/s and strain $\gamma = 0.5\%$; (2) an amplitude sweep at $\omega = 3.14$ rad/s, exploring the strain range from 0.01 to 100%; (3) time sweep for 3 h at $\omega = 3.14$ rad/s and $\gamma = 0.5\%$; (4) frequency sweep at $\gamma = 0.5\%$, exploring the frequency range from 0.01 to 100 rad/s. A similar protocol was performed for PDMS−NH_2, but a constant strain of $\gamma = 0.3\%$ is used for both time and frequency sweeps. $t = 0$ in the presented data corresponds to the beginning of conditioning oscillations.

Dynamic Light Scattering. DLS measurements were performed on a Malvern Zetasizer Nano ZS equipped with a 633 nm laser at a scattering angle of 90°.

RESULTS

NPS Assembly. The aqueous phase in our experiments contained 1 mg mL^{-1} and 14 nm diameter of −COOH− functionalized silica NPs. For the nonpolar phase, we used a low-viscosity (kinematic viscosity 5 cSt, $\rho = 912$ kg m^{-3}) silicone oil containing NH_2-functionalized PDMS-based polymer surfactants. Three different NH_2-functionalized

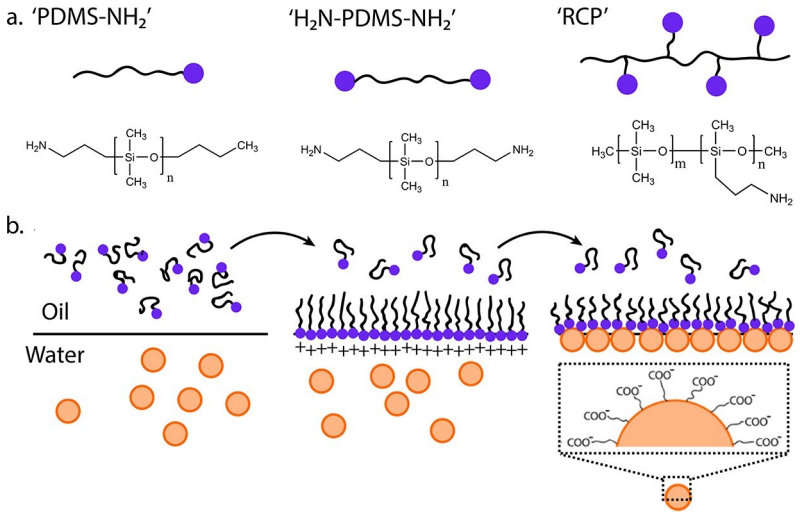

Figure 1. Assembly mechanism of NPSs. (a) Amine-functionalized polymer surfactants used in this study. (b) During NPS formation, polymer surfactants first adsorb to the interface and protonate, attracting the Si−COOH NPs to the oil−water interface. Interaction between the particles and the polymer surfactant renders the particles irreversibly bound to the interface. A similar interaction occurs among the NPs, double amine-terminated $H_2N-PDMS-NH_2$, and an amine-functionalized "RCP", but with the potential for cross-link formation.

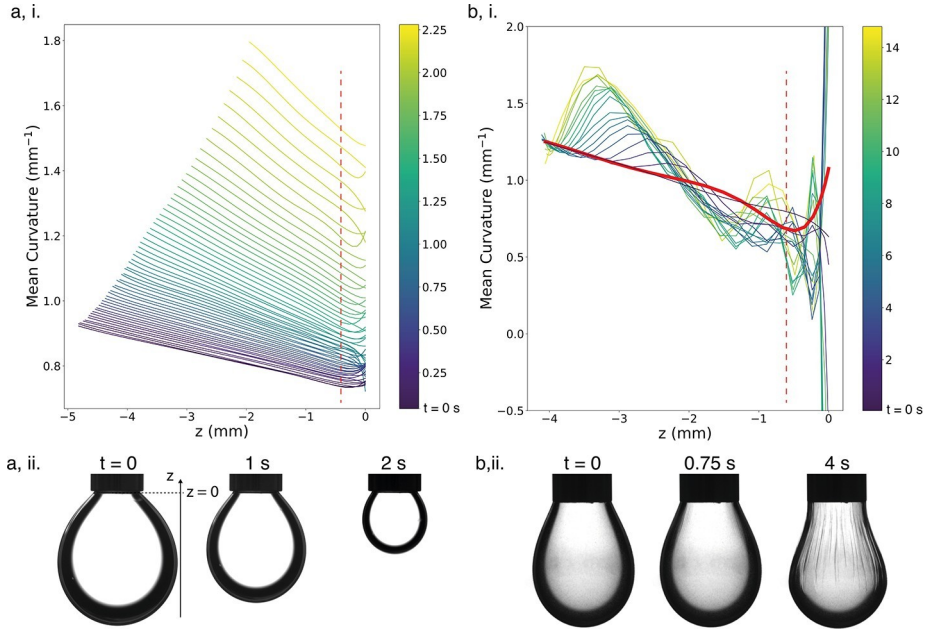

Figure 2. Isotropic and anisotropic surface stresses in a model system. Water is withdrawn from a droplet suspended from a needle and immersed in oil. (a) Aqueous phase contains 5 mM NaMES and nonaqueous phase contains silicone oil. (b) 5 mM NaMES and 1 mg mL^{-1} Si NPs, nonaqueous phase contains silicone oil + 5% w/w $PDMS-NH_2$. (i) Mean curvature of the oil−water interface as a function of both time (indicated by color) and distance from the apex of the droplet (defined in a, ii) when the interface is compressed. The red dashed line shows the distance over which anisotropic surface stresses due to the needle decay. The solid red line indicates the time point at which interface solidification was detected (0.75 s). (ii) Images of the droplets as the interface is compressed.

polymer surfactants were chosen that differ in the number of amine-functional groups and structure (Figure 1a). PDMS− NH_2 has one primary amine; $H_2N-PDMS-NH_2$ is capped on both ends with primary amines and the amine-functionalized RCP has multiple amine groups per molecule. The relative concentrations of polymer surfactants used in this work are shown in Table S1. Below a critical pH, the amine moiety protonates and the polymer surfactant becomes surface active, forming a positively charged monolayer.[31−33] The negatively charged NPs interact electrostatically with the protonated amine-functionalized ligands, resulting in the formation of

NPSs that are irreversibly bound to the oil−water interface (schematic, Figure 1b). The particle monolayer is extremely strongly bound to the oil−water interface and, when compressed, it will jam into a solid-like layer that supports anisotropic surface stresses.[7,16] It is important to note that, in this work, we used particles that do not spontaneously adsorb to the oil−water interface. As such, the surface tension of the oil−water interface in the absence of the polymer surfactant is constant over time (Figure S1). If a polymer surfactant is present in the nonaqueous phase, the surface tension of the oil−water interface will drop, but, in the absence of NPs in the

aqueous phase, the polymer surfactant is not sufficiently strongly bound to the oil−water interface to support anisotropic surface stresses, and so, pendant drops in this case do not wrinkle when compressed (Figure S2). If both NPs are present in the aqueous phase and the polymer surfactant is present in the nonaqueous phase, the surface tension of the oil−water interface is lower than that observed because of only the polymer surfactant being present and, when compressed, the interface will buckle as the irreversibly adsorbed NPS assembly solidifies.

Surface Stress Anisotropy Measurements. The pendant drop method was used to study the assembly and solidification of the NPS at the oil−water interface. The shape of the pendant drop suspended from a capillary inside the second fluid is described by the Young−Laplace equation

$$\gamma_{ij}\left(\frac{1}{R_1}+\frac{1}{R_2}\right)=P_0-\Delta\rho g z \quad (2)$$

where R_1 and R_2 are the principal curvatures of the oil−water interface, P_0 is the pressure difference between the two phases at $z = 0$, $\Delta\rho$ is the density difference between the two liquids, g is the acceleration due to gravity, and z is the vertical distance from the tip of the capillary (Figure 2a(i)). In the case of surface stresses at the oil−water interface being isotropic (i.e., $\Gamma_{ij} = 0$), the mean curvature of the interface varies linearly with distance from the apex of the droplet, that is, $H = \left(\frac{1}{R_1}+\frac{1}{R_2}\right) \propto z$. As a model system for this case, we initially studied pendant drops containing 5 mM solution of NaMES immersed in silicone oil (Figure 1b). Note that surface stress anisotropy was seen near the needle from which the droplet was suspended because of wetting effects. These stresses were observed to decay on a length scale of approximately 0.5 mm (red-dashed lines, Figure 1a,b), and so, only regions of the droplet farther from the needle than this were analyzed in this work. Away from the region in which the needle deformed the droplet, H could be clearly seen to be linear with distance from the apex of the droplet, when the interface was compressed. As a model system that exhibited anisotropic surface stresses, we then studied a droplet in which the aqueous phase contained 1 mg mL^{-1} silica NPs in a bath of silicone oil containing 5% w/w PDMS−NH_2. The droplet was immersed in the bath for 2 h, allowing NPSs to assemble. Water was then slowly withdrawn from the droplet, and the mean curvature of the oil−water interface was monitored. Initially, $H \propto z$, showing that surface stresses in the droplet were isotropic. However, upon compression, H became strongly nonlinear with z, indicating the

NPS assembly in the presence of PDMS−NH_2, H_2N−PDMS− NH_2, and RCP (Figure 3). The concentration of the polymer surfactant in the nonpolar phase was 5% w/w in all cases, while particle concentration in the aqueous phase was 1 mg mL^{-1}.

The observed behavior depended strongly on the polymer surfactant used to assemble the NPs at the oil−water interface. In the presence of PDMS−NH_2, the droplet was seen to elongate over time, indicating a reduction in the surface tension due to the NPS assembly, but no interfacial solidification was observed on the experimental timescale (2 h) (Figure 3a). Significantly different behavior was observed in the presence of polymer surfactants that bore multiple-NH_2 groups, and so have the potential to form cross-linked assemblies (Figure 3b,c). On short timescales, the mean curvature of the interface was linear with z. On longer timescales, significant interfacial solidification was observed without compression of the interface, indicating

PDMS−NH_2 typically produced solidified interfaces in approximately 10 min, while using RCP, which bears a larger number of NH_2 groups, leads to rapid interfacial solidification (on the order of minutes). The case of RCP is particularly noteworthy, in that within 10 minutes, the droplet had spontaneously adopted a highly nonequilibrium, asymmetric shape (Figure 3c(ii)). The time evolution of the system then depended on the polymer surfactant. The H_2N−PDMS−NH_2- based NPS exhibited little time evolution after interfacial solidification. By contrast, droplets at which RCP-based NPS solidification of the interface (Figure 1b).[34−36] We then measured the time point at which surface stresses became anisotropic by calculating the spatial derivative of H and defined the solidification timescale as the time point at which the dimensionless coefficient of variation of H', $c_v = \frac{\sigma_{H'}}{}$ (i.e., the standard deviation of H'

were assembled exhibited a significant change in the structure after interfacial solidification, with the droplets becoming highly asymmetric and the curvature of the interface changing enormously. We attribute this difference in ageing behavior to the different bending moduli of the assemblies, which we return to in the section on spontaneous wrinkling of the pendant drops.

Pendant Drop Tensiometry. We then extended our analysis of pendant drops to a wider range of polymer surfactant concentrations, using the emergence of anisotropic surface stress to measure the timescale of interfacial solidification, τ, and hence, it determines the timescale on which

divided by its mean), rose above an empirically determined threshold (see the Materials and Methods section and Figures S3−S5). The time point at which the interface solidified is indicated by the red solid line in Figure 2b(i), and the droplet imaged at 0.75 s is shown in Figure 2b(ii).

We then applied this principle to pendant drops at which NPSs were assembling to study the solidification of the assembly without compression. To do this, we measured the mean curvature of pendant drops as a function of time during

interfacial tension could be extracted using the Young−Laplace equation. For PDMS−NH_2 and H_2N−PDMS−NH_2, polymer concentrations of 0.5, 1, and 5% w/w were studied. For the RCP, a far broader range of behavior was observed, and further experiments were performed at 0.01 and 0.1% w/w. In all cases, three separate regimes in dynamic interfacial tension were seen (Figure 4). First, an extremely rapid decrease in surface tension occurred (more rapid than can be detected by the experimental apparatus), and so, the initially measured surface tension is significantly smaller than that of a bare silicone oil−water interface. The system then enters a diffusion-limited regime of reduction in interfacial tension.

Both the size of the initial rapid reduction and the rate of the diffusion-limited change in $\gamma(t)$ increase with surfactant concentration in all cases. Finally, either interfacial tension was observed to plateau or, at higher concentrations in cross-linked assemblies, interfacial solidification was observed (red stars, Figure 4).

The timescales on which the system exhibited these three regimes depended on both the concentration and structure of the polymer surfactant. At low polymer surfactant concentrations (0.01 and 0.1% RCP, 0.5% PDMS−NH_2 and H_2N−

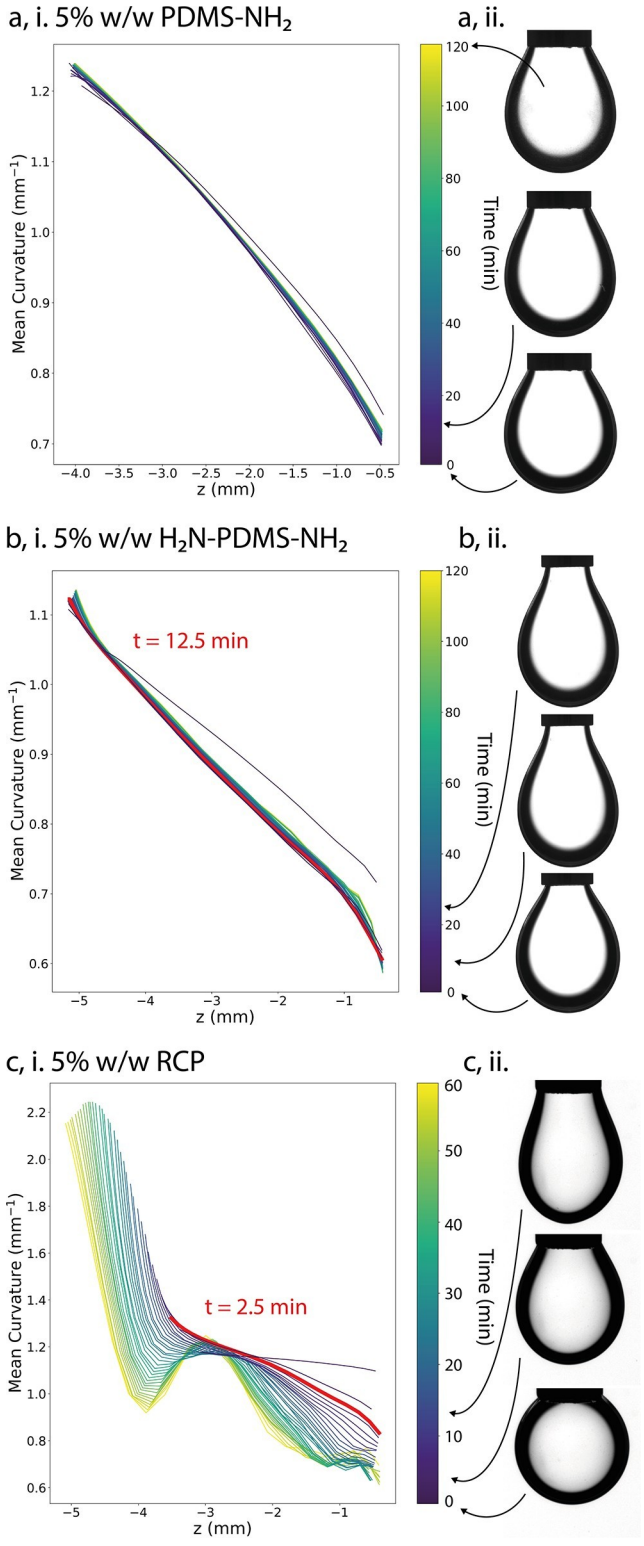

Figure 3. Solidification of droplet interfaces in the presence of self- assembling NPSs. (a) Pendant drops of aqueous solution of MES (5 mM) containing 14 nm diameter Si NPs (1 mg mL^{-1}) imaged at time, *t*, after immersion in a bath of silicone oil containing (a) PDMS−NH_2, (b) H_2N−PDMS−NH_2, and (c) RCP (all 5% w/w). (b) Mean curvature of the droplets as a function of distance from the tip of the capillary, *z*, and time (denoted by colored lines). The red line indicates the

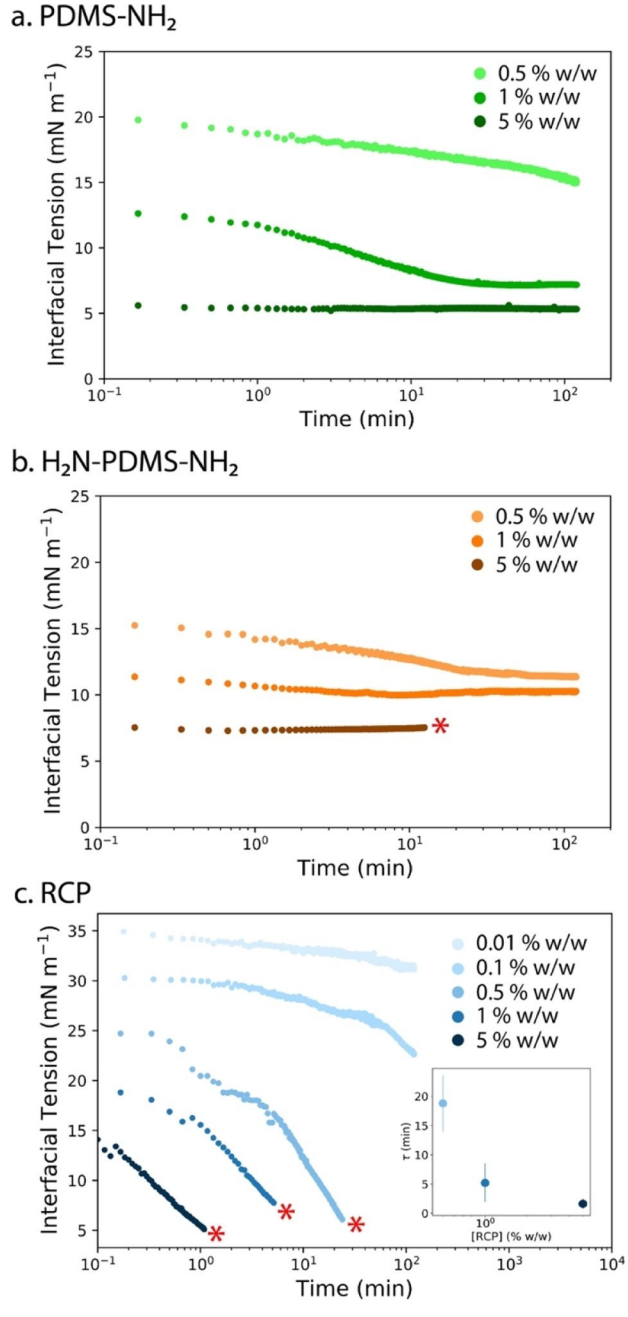

Figure 4. Surface tension of oil−water interfaces at which NPSs are assembling. Aqueous phase contains 1 mg mL^{-1} silica NPs in 5 mM NaMES at pH 6.4. The nonpolar phase is silicone oil containing the stated concentrations of (a) PDMS−NH_2 (green), (b) H_2N−PDMS−NH_2 (orange), and (c) RCP (blue) in silicone oil. Red asterisks denote the data that have been truncated because of interfacial solidification. (c, inset) Interfacial solidification timescale as a function of polymer surfactant concentration. Error bars are 1 standard deviation, $n = 3$.

PDMS−NH_2), the diffusion-limited region was not seen to end on the experimental timescale (in some cases as long as 18 h). As polymer surfactant concentration was increased, the interfacial tension was observed to plateau without the system exhibiting interfacial solidification (i.e., 1% w/w, 5% w/w polymeric H_2N−PDMS−NH_2, and 1% w/w H_2N−PDMS−NH_2). As time point at which the interface solidified.

surfactant concentration was increased further, polymer surfactants bearing multiple amine groups formed cross-linked assemblies, resulting in interfacial solidification (Figure 4b,c).

The RCP spontaneously formed solid interfaces over a broad range of polymer concentrations, allowing trends in τ to be studied. This timescale decreased extremely rapidly with increasing the polymer surfactant concentration, from 18.8 ± 4.7 min at 0.5% w/w RCP, to 1.1 ± 0.8 min at 5% w/w RCP (Figure 4c, inset). This can be explained by considering the timescale on which the NPSs can rearrange on the surface of the droplet versus the effective strain rate on a hoop section of the pendant drop caused by the reduction in surface tension. As polymer surfactant concentration is increased, NPSs form more rapidly and surface tension reduces more quickly. This gives NPS rafts less time to rearrange to relax anisotropic surface stresses, which means that the interface jams more rapidly.

The areal density of particles in the NPS assembly was then estimated using a compression assay.[24,37] After measuring the surface tension, the aqueous phase was slowly withdrawn from the droplet (10 μL min^{-1}). Withdrawing the aqueous phase reduces the volume of the droplet and hence, decreases the surface area of the droplet. This compresses the interface and therefore, increases the particle density. Because the NPSs do not desorb from the interface, when the NPSs jam or close- pack, the interface buckles out-of-plane. In all cases, with- drawing the aqueous phase led to wrinkling of the droplets, indicating the presence of a solid NPS film at the oil−water interface. After sufficiently long time (on the order of minutes at 5% w/w, and approximately 3 h at 0.5% w/w), extremely small compressions (i.e., smaller than the detection limit of equipment) were found to induce wrinkling in the droplets, suggesting near close-packing of the particles at the interface, regardless of polymer surfactant concentration, in agreement with the observations made using in situ AFM by Chai et al.[38] Interfacial solidification was observed in all systems, either spontaneously or in response to negligible compressions of the oil−water interface. This occurred over a range of interfacial tensions, from 1 to 15 mN m^{-1}. This is somewhat counter-intuitive given that, in NP-only systems, the number density of NPs at the interface, n, can be estimated from the surface pressure using the relation $\Pi(n) = n\Delta E$, where ΔE is the interfacial binding energy per particle.[39,40] There are several reasons for the breakdown of this relation in our system. First, the relation $\Pi(n) = n\Delta E$ fails at high particle densities as particle−particle interactions contribute directly to the surface pressure.[41,42] This factor is particularly important in our system at timescales on which the NPS assemblies become solid-like. The multicomponent nature of the systems causes two further deviations: surface excess of the polymer surfactant increases with concentration, causing a reduction in γ.[41] Finally, the wetting characteristics (i.e., the contact angle) of the particles due to binding of the polymer surfactants to the NPs are dependent on polymer concentration, as can be inferred from concentration-dependent phase inversion of NPS-stabilized emulsions (Figure S6).

It is important to note that, somewhat counterintuitively, the three regimes of dynamic surface tension seen in this work were accessed most rapidly by the highest molecular weight polymer (i.e., the RCP). The RCP has a molecular weight over four times greater than the other two polymers used and therefore, a two-fold lower diffusion coefficient and four-fold lower molar concentration (4.5 mM vs 20 and 25 mM at 5% w/w for $PDMS{-}NH_2$ and $H_2N{-}PDMS{-}NH_2$, respectively, see Supporting Information, Table 1).[43−45] Despite this, it proved to be remarkably effective in reducing interfacial

tension and driving interfacial solidification at far lower concentrations than both PDMS−NH_2 and H_2N−PDMS− NH_2. This unintuitive difference in the observed kinetics of the system becomes more marked when the dynamic interfacial tensions are rescaled by the diffusion coefficients of the polymer surfactants (Figure S7).[44,45] The effect of both polymer surfactant concentration and molecular weight upon dynamic surface tension of NPS assemblies has been investigated extensively by Huang et al.[46] The findings we present here are consistent with their observations that higher molecular weight polymers lead to lower interfacial tensions and that, more intuitively, increasing the polymer concen- tration accelerates NPS formation kinetics. Our results extend this analysis and point to the important role played by polymer structures and functional group density in controlling the kinetics of the NPS assembly. While the current work focuses on an application-oriented system that is used in all-liquid 3D printing (and, hence, conditions and concentrations relevant to that body of work),[5] future work must explore the importance of polymer structures and the role that adsorbed density of functional groups and adsorption barriers due to polymer conformation in solvent play in determining NPS formation kinetics.

Spontaneous Wrinkling of Droplets at Low Surface Tension. On longer timescales, the RCP-based NPS assemblies were found to spontaneously wrinkle without the withdrawal of the aqueous phase (Figure 5). This occurred because of extensional stresses acting on the droplet, which is due to the density difference between the two liquids and the surface energy of the system reaching extremely low values. Gravitational stresses stretch the droplet interface axially,

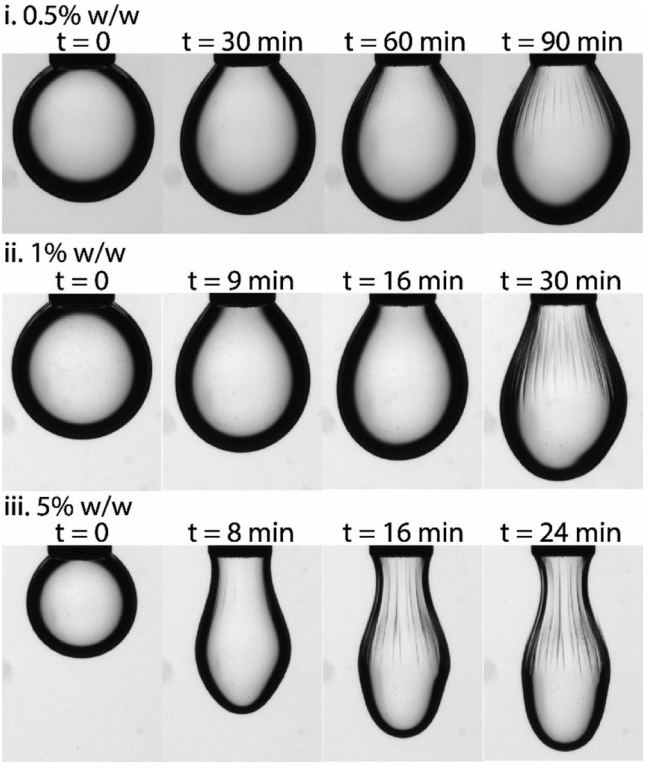

Figure 5. Spontaneous wrinkling of aqueous pendant drops without water extraction. Pendant drops containing 1 mg mL^{-1} silica NPs in silicone oil containing (i) 0.5, (ii) 1, and (iii) 5% w/w RCP extend and wrinkle as the oil−water surface tension reduces.

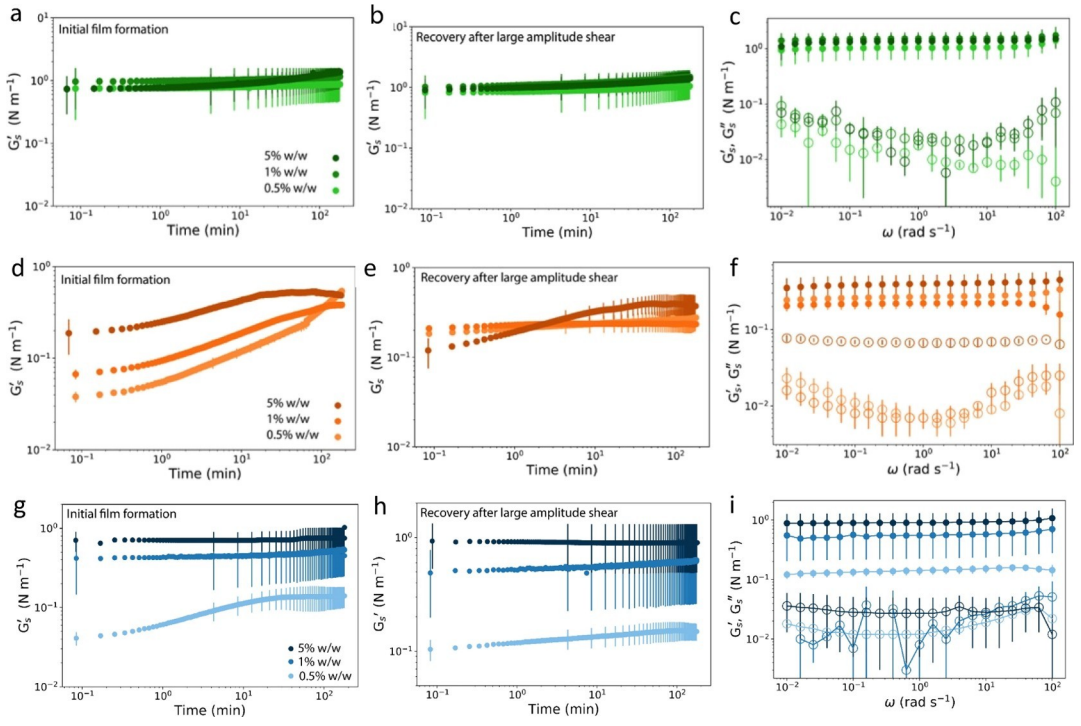

Figure 6. Small amplitude oscillatory interfacial shear rheology of NPSs assembling at the oil−water interface. (a−c, green) PDMS−NH_2, (d−f, orange) H_2N−PDMS−NH_2, and (g−i, blue) RCP. (a,d,g) Evolution of viscoelastic moduli as the NPSs assemble over time. Three different concentrations of amine-functionalized polymers are shown: 5, 1, and 0.5%. Error bars show the standard deviation in three measurements. (b,e, and h) Recovery of the viscoelastic moduli after large amplitude plastic deformation. (c, f, and i) Viscoelastic moduli as a function of frequency after film formation. G'_s = closed symbols, G''_s = open symbols.

causing a compressive hoop stress to act on the NPS film.[47,48] The bending modulus of the RCP-based NPS film has been measured elsewhere to be rather small, of the order 10 kT.[5] By contrast, as shown later, the shear modulus of the assemblies studied here is comparatively large, 0.1−1 N m^{-1}. The compressive modulus, E, of the system can be estimated using the relation $E = 2G(1 + \nu)/d$. Literature values of the Poisson ratio, ν, for a 2D array of hard spheres differ, with values of $\nu = 1/3$ and $1/\sqrt{3}$ being reported.[49−51] Taking these values into account allows us to place an estimate on the 2D compressive modulus of $E \approx 0.19-2.2$ MPa, depending on the shear modulus of the assemblies. The large compressive modulus and the extremely low bending modulus of the films mean that, even extremely small compressive stresses cause wrinkling in close-packed NPS assemblies.

While the Young−Laplace equation is clearly inappropriate for analyzing the system under these circumstances, the z-component of the surface stress can be estimated by measuring the maximum volume of water droplet that can be suspended from the needle without detaching from the capillary (approximately 5 mL for 5% w/w RCP, see Figure S8). A force balance between gravitational and surface stresses in the direction of the z-axis just prior to detachment yields $\tau_{zz} = \Delta\rho V_{drop} g/2\pi r$. This gives $\tau_{zz} \approx 1$ mN m^{-1}, which is significantly lower than the interfacial tension prior to solidification as shown by the red asterisks in Figure 4. This shows that the shape evolution of the pendant drop on longer timescales is governed by both surface energy and the

extensional forces of the NPS-coated pendant drops comes from the surface energy of the oil−water interface and not from the mechanical properties of the NPS assembly. This is in contrast to capsules formed by interfacial polymerization or polyelectrolyte−polyelectrolyte complexation, in which the highly cross-linked coacervate films arrest the detachment of a pendant droplet from a needle even at extremely low surface tension.[52] We are currently investigating how the stress history of the sample, due to, for instance, jamming of assemblies of attractive particles into a coherent film by small compressions, affects this behavior.

Interfacial Shear Rheology of NPS Assemblies. Having quantified the timescales on which NPS assemblies solidify and how this mechanical properties of the NPS film. This also highlights an interesting difference between capsules and NP-coated pendant drops. Prior to solidification, the NPS assemblies consist of a liquid-like ensemble of discrete NPs. Resistance to is determined by polymer surfactant concentration, the shear rheology of NPS films was then studied using a double-wall ring geometry attached to a commercial rheometer. Stresses and strains in the NPS assembly are then related by the complex shear modulus, G^*_s, which can be decomposed into the surface storage modulus, G'_s and the surface loss modulus, G''_s. We restricted our experiments to NPS systems that formed close-packed assemblies on the experimental timescale (i.e., all systems studied in this work apart from that with 0.01 and 0.1% w/w RCP), so that the effect of the polymer surfactant, rather than particle density, on the mechanical properties of the assemblies could be investigated.

At all polymer surfactant concentrations studied, NPS assemblies rapidly led to the formation of a solid-like layer, where G'_s is greater than G''_s (Figure 6a-c: PDMS−NH_2, 6d-f: H_2N−PDMS−NH_2 and 6g-i: RCP). G'_s was typically found to be 2 orders of magnitude greater than G''_s (phase angle, $\delta \approx 0$). As such, the observed surface loss modulus may be due to

noise or sub-phase contributions (we therefore only for G''_s when commenting explicitly on them). The evolution of the rheological moduli depended strongly on the structure and size of the polymer surfactant. The storage moduli of $H_2N-PDMS-NH_2$ and RCP films grew on a timescale that varied from minutes to hours, depending on surfactant concentration, eventually reaching a plateau value (Figure 6d,g). For instance, at concentrations of 1 and 5% w/w RCP, the film is formed in less than a minute, whereas for 0.5% w/w RCP, it took almost 50 min for G'_s to reach its plateau value (Figure 6g). In addition, the initial and plateau values of G'_s increased with polymer concentration.

It is also notable that the pendant drops do not solidify on extremely small timescales, even though the interfacial shear rheology measurements are elastic-dominated even for extremely short periods of time. This can be rationalized by considering that the area of the pendant drop is not constant with time (even when the interface has solidified in places, as shown in Figure 3). As the surface tension decreases in the pendant drop, the amount of surface area increases. The geometry of the pendant drop means that some regions of the oil−water interface expand (particles in this region can undergo thermal rearrangement) and others contract. In contrast to the pendant drop method, the amount of surface area is constant in the interfacial shear rheology measurements. This prevents any such rearrangements once the interface has solidified. Further evidence for this thermal relaxation of anisotropic surface stresses in pendant drops, prior to interfacial solidification, was also observed directly. Non-monotonic variations in the degree of surface stress anisotropy in the pendant drops studied in Figure 2 show that local variations in surface stresses can be relaxed prior to interfacial solidification (Figure S5).

After rupturing the NPS films using large amplitude oscillatory shear, a new time sweep experiment was performed to observe the layer reformation over time (Figure 6b: $PDMS-NH_2$, 6e: $H_2N-PDMS-NH_2$ and 6h: RCP). The NPS films respond to this plastic deformation by self-healing, with the rate of recovery of the moduli being similar to the rate of their increase in the initial formation experiment (Figure 6b,e,h). The viscoelastic moduli showed no significant dependence on the frequency of oscillation, ω, with the film exhibiting solid-like behavior on all timescales for all the three NH_2-functionalized polymer surfactants (Figure 6c: $PDMS-NH_2$, 6f: $H_2N-PDMS-NH_2$ and 6i: RCP).

Along with probing the shear moduli of

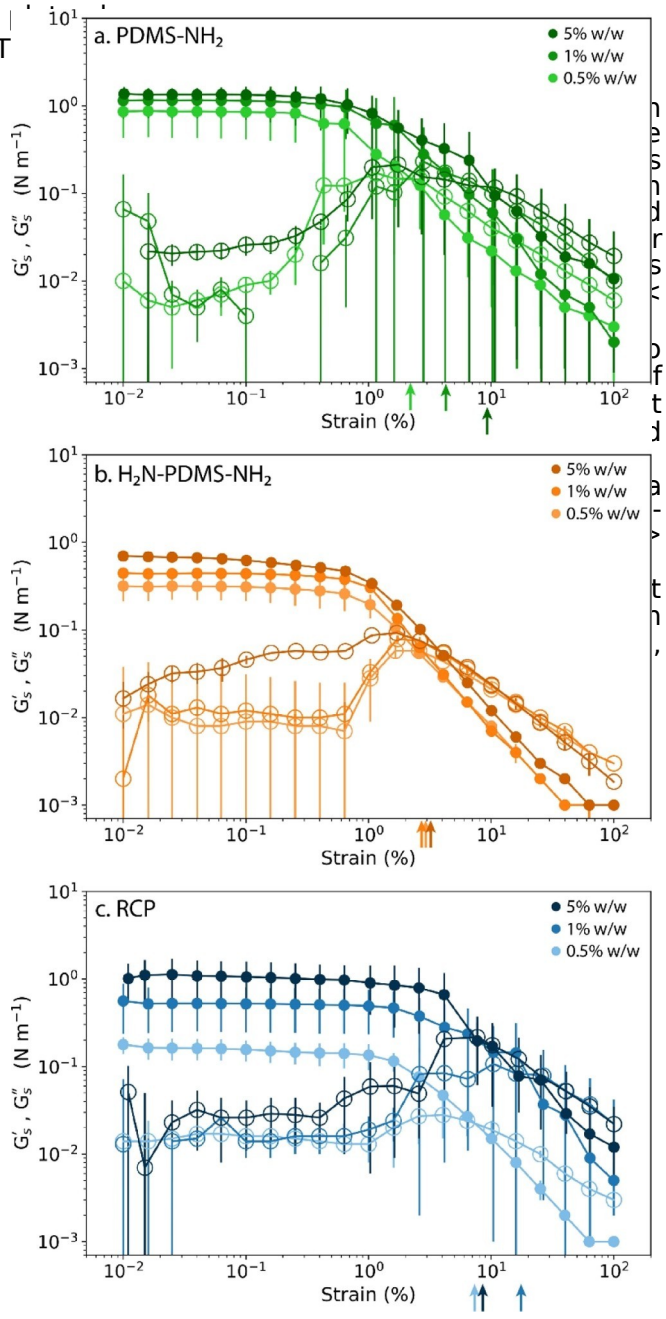

$H_2N-PDMS-NH_2$ and RCP showed the greatest concen-

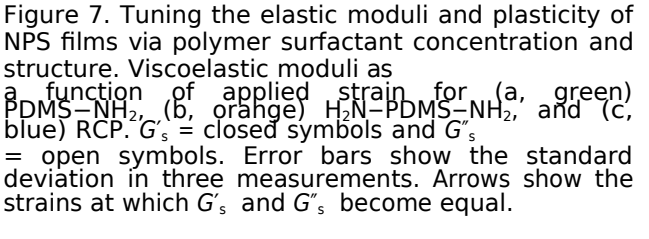

Figure 7. Tuning the elastic moduli and plasticity of NPS films via polymer surfactant concentration and structure. Viscoelastic moduli as a function of applied strain for (a, green) $PDMS-NH_2$, (b, orange) $H_2N-PDMS-NH_2$, and (c, blue) RCP. G'_s = closed symbols and G''_s = open symbols. Error bars show the standard deviation in three measurements. Arrows show the strains at which G'_s and G''_s become equal.

The values of the storage moduli in the linear regime of the NPS assemblies were found to vary by an order of magnitude with polymer concentration and structure, with all values lying in the range 0.1−1 N m^{-1} (Figure 7). These values are comparable to those obtained for silica particle monolayers that are either spread at, or adsorbed spontaneously to the liquid−fluid interface.[22,23,53] G'_s in $PDMS-NH_2$-based NPS films (Figure 7a) had a storage modulus of approximately 1 N m^{-1}, regardless of polymer concentration. By contrast, both

tration dependence (Figure 7b,c). This rather small variation in G'_s suggests that the storage moduli of the NPS films are determined largely by the particle density in close-packed NPS assemblies, and that polymer cross-links ect the shear modulus only to a limited degree. This also suggests that LB-trough- based methods for measuring the shear modulus, which yield rather small estimates for the shear modulus of particle layers, become rather poor at high areal particle densities, likely because of the complex stress fields in solid Langmuir layers.[54,55]

Altering the polymer surfactant structure appears to lead to structural changes that weakly alter the shear modulus. This may be due to the generation of frustrated structures caused by short-ranged, strongly attractive interactions due to cross-links formed by polymers with multiple functional groups or may be a kinetic effect due to the quantity of particles that adsorb during the initial rapid phase. We are currently applying in situ AFM methods to confirm these hypotheses.

CONCLUSIONS

The formation kinetics and mechanical properties of NPSs assembled at the oil−water interface have been studied. Increasing the concentration of a hydrophobic, amine-functionalized PDMS polymer rapidly accelerates the assembly of NPSs at the oil−water interface. Image analysis techniques showed that polymer surfactants containing multiple functional groups and, hence, that are capable of forming cross-links, produce NPS assemblies that spontaneously solidify. Remarkably, after interfacial solidification, pendant drops continued to evolve with time and, at sufficiently low surface tensions, they were seen to spontaneously wrinkle. The shear modulus of the NPS assemblies was found to vary from 0.1 to 1 N m^{-1}, comparable to values of shear moduli obtained for NP monolayers spread at the liquid−fluid interface. Our work adds to the growing canon of literature studying the origins of the mechanical properties of NP assemblies.[22,23,55−58] Our results suggest two fruitful avenues of future work. First, given the wealth of particles and polymer surfactants from which NPS can be made and tunability of the mechanical moduli of NPS films, designer interfaces must be constructed that allow us to tune the functionality and mechanical properties of the printed and molded structures that these systems can be used to generate. Second, the relationship between the shear and bending moduli of these highly tunable assemblies must be investigated. In particular, altering the molecular weight of the polymer surfactants that comprise the NPS should result in the ability to alter the bending moduli and shear moduli independently of one another.

AUTHOR INFORMATION

Corresponding Author

*E-mail: russell@mail.pse.umass.edu.

ORCID

Anju Toor: 0000-0002-8613-7547

Simone Bochner de Araujo: 0000-0003-4967-5781

Yu Chai: 0000-0001-6085-4321

Paul D. Ashby: 0000-0003-4195-310X

Thomas P. Russell: 0000-0001-6384-5826

Author Contributions

○ A.T. and J.F. contributed equally to this article.

Notes

The authors declare no competing financial interest.

ACKNOWLEDGMENTS

This work was supported by the U.S. Department of Energy, Office of Science, Basic Energy Sciences under contract no. DE-AC02-05-CH11231 within the Adaptive Interfacial Assem- blies Toward Structuring Liquids program (KCTR16) and the user program at the Molecular Foundry. We thank Gregory Grason for useful discussion.

REFERENCES

(1) Montelongo, Y.; Sikdar, D.; Ma, Y.; Mcintosh, A. J. S.; Velleman, L.; Kucernak, A. R.; Edel, J. B.; Kornyshev, A. A. Electrotunable Nanoplasmonic Liquid Mirror. *Nat. Mater.* 2017, *16*, 1127−1135.

(2) Gu, X. W.; Ye, X.; Koshy, D. M.; Vachhani, S.; Hosemann, P.;
Alivisatos, A. P. Tolerance to Structural Disorder and Tunable Mechanical Behavior in Self-Assembled Superlattices of Polymer- Grafted Nanocrystals. *Proc. Natl. Acad. Sci. U.S.A.* 2017, *114*, 2836−2841.

(3) Fang, P.-P.; Chen, S.; Deng, H.; Scanlon, M. D.; Gumy, F.; Lee,
H. J.; Momotenko, D.; Amstutz, V.; Corteś-Salazar, F.; Pereira, C. M.;
Yang, Z.; Girault, H. H.; Scanlon, D.; Fang, P.-P.; Chen, S.; Deng, H.; Pereira, C. M.; Yang, Z. Conductive Gold Nanoparticle Mirrors at Liquid/Liquid Interfaces. *ACS Nano* 2013, *7*, 9241−9248.

(4) Huang, C.; Forth, J.; Wang, W.; Hong, K.; Smith, G. S.; Helms,
B. A.; Russell, T. P. Bicontinuous structured liquids with sub- micrometre domains using nanoparticle surfactants. *Nat. Nanotechnol.* 2017, *12*, 1060−1063.

(5) Forth, J.; Liu, X.; Hasnain, J.; Toor, A.; Miszta, K.; Shi, S.;
Geissler, P. L.; Emrick, T.; Helms, B. A.; Russell, T. P. Reconfigurable Printed Liquids. *Adv. Mater.* 2018, *30*, 1707603.

(6) Reeves, M.; Brown, A. T.; Schofield, A. B.; Cates, M. E.; Thijssen, J. H. J. Particle-Size Effects in the Formation of Bicontinuous Pickering Emulsions. *Phys. Rev. E: Stat., Nonlinear, Soft Matter Phys.* 2015, *92*, 032208.

(7) Cui, M.; Emrick, T.; Russell, T. P. Stabilizing Liquid Drops in Nonequilibrium Shapes by the Interfacial Jamming of Nanoparticles. *Science* 2013, *342*, 460−463.

(8) Zhang, Z.; Jiang, Y.; Huang, C.; Chai, Y.; Goldfine, E.; Liu, F.;

Feng, W.; Forth, J.; Williams, T. E.; Ashby, P. D.; Russell, T. P.; Helms, B. A. Guiding kinetic trajectories between jammed and unjammed states in 2D colloidal nanocrystal-polymer assemblies with zwitterionic ligands. *Sci. Adv.* 2018, *4*, No. eaap8045.

(9) Chai, Y.; Lukito, A.; Jiang, Y.; Ashby, P. D.; Russell, T. P. Fine- Tuning Nanoparticle Packing at Water-Oil Interfaces Using Ionic Strength. *Nano Lett.* 2017, *17*, 6453−6457.

(10) French, D. J.; Taylor, P.; Fowler, J.; Clegg, P. S. Making and breaking bridges in a Pickering emulsion. *J. Colloid Interface Sci.* 2015, *441*, 30−38.

(11) Toor, A.; Helms, B. A.; Russell, T. P. Effect of Nanoparticle Surfactants on the Breakup of Free-Falling Water Jets during Continuous Processing of Reconfigurable Structured Liquid Droplets. *Nano Lett.* 2017, *17*, 3119−3125.

(12) Sun, Z.; Feng, T.; Russell, T. P. Assembly of Graphene Oxide at Water/Oil Interfaces: Tessellated Nanotiles. *Langmuir* 2013, *29*, 13407−13413.
(13) Feng, T.; Hoagland, D. A.; Russell, T. P. Assembly of Acid-
Functionalized Single-Walled Carbon Nanotubes at Oil/Water Interfaces. *Langmuir* 2014, *30*, 1072−1079.
(14) Liu, X.; Shi, S.; Li, Y.; Forth, J.; Wang, D.; Russell, T. P. Liquid
Tubule Formation and Stabilization Using Cellulose Nanocrystal Surfactants. *Angew. Chem., Int. Ed.* 2017, *56*, DOI: 10.1002/ anie.201706839
(15) Huang, C.; Chai, Y.; Jiang, Y.; Forth, J.; Ashby, P. D.; Arras, M.
M. L.; Hong, K.; Smith, G. S.; Yin, P.; Russell, T. P. The Interfacial Assembly of Polyoxometalate Nanoparticle Surfactants. *Nano Lett.* 2018, *18*, 2525−2529.
(16) Cui, M.; Miesch, C.; Kosif, I.; Nie, H.; Kim, P. Y.; Kim, H.;
Emrick, T.; Russell, T. P. Transition in Dynamics as Nanoparticles Jam at the Liquid/Liquid Interface. *Nano Lett.* 2017, *17*, 6855−6862.
(17) Hermans, E.; Saad Bhamla, M.; Kao, P.; Fuller, G. G.; Vermant,
J. Lung Surfactants and Different Contributions to Thin Film Stability. *Soft Matter* 2015, *11*, 8048−8057.
(18) Sagis, L. M. C. Dynamic Properties of Interfaces in Soft Matter: Experiments and Theory. *Rev. Mod. Phys.* 2011, *83*, 1367−1403.
(19) Nagel, M.; Tervoort, T. A.; Vermant, J. From Drop-Shape Analysis to Stress-Fitting Elastometry. *Adv. Colloid Interface Sci.* 2017, *247*, 33−51.
(20) Sagis, L. M. C. Rheology of Complex Fluid-Fluid Interfaces: A
Unified Approach Based on Nonequilibrium Thermodynamics. *Appl. Rheol.* 2010, *20*, 24380.
(21) Zang, D. Y.; Rio, E.; Langevin, D.; Wei, B.; Binks, B. P. Viscoelastic Properties of Silica Nanoparticle Monolayers at the Air- Water Interface. *Eur. Phys. J. E* 2010, *31*, 125−134.
(22) Maestro, A.; Zaccone, A. Nonine deformation and tunable
yielding of colloidal assemblies at the air-water interface. *Nanoscale*
2017, *9*, 18343−18351.
(23) Maestro, A.; Deshmukh, O. S.; Mugele, F.; Langevin, D.
Interfacial Assembly of Surfactant-Decorated Nanoparticles: On the Rheological Description of a Colloidal 2D Glass. *Langmuir* 2015, *31*, 6289−6297.
(24) Shi, S.; Liu, X.; Li, Y.; Wu, X.; Wang, D.; Forth, J.; Russell, T. P.
Liquid Letters. *Adv. Mater.* 2018, *30*, 1705800.
(25) Forth, J.; Kim, P. Y.; Xie, G.; Liu, X.; Helms, B. A.; Russell, T.
P. Building Reconfigurable Devices Using Complex Liquid-Fluid Interfaces. *Adv. Mater.* 2019, *31*, 1806370.
(26) Vitantonio, G. D.; Wang, T.; Haase, M. F.; Stebe, K. J.; Lee, D. Robust Bijels for Reactive Separation via Silica-Reinforced Nano- particle Layers. *ACS Nano* 2019, *13*, 26−31.
(27) Haase, M. F.; Sharifi-Mood, N.; Lee, D.; Stebe, K. J. In Situ
Mechanical Testing of Nanostructured Bijel Fibers. *ACS Nano* 2016,
10, 6338−6344.
(28) Boakye-Ansah, S.; Schwenger, M. S.; Haase, M. F. Designing
Bijels Formed by Solvent Transfer Induced Phase Separation with Functional Nanoparticles. *Soft Matter* 2019, *15*, 3379−3388.
(29) Xing, K.; Tress, M.; Cao, P.; Cheng, S.; Saito, T.; Novikov, V.
N.; Sokolov, A. P. Hydrogen-Bond Strength Changes
Network Dynamics in Associating Telechelic PDMS. *Soft Matter* 2018, *14*, 1235−1246.
(30) Kataoka, T.; Ueda, S. Viscosity-Molecular Weight Relationship
for Polydimethylsiloxane. *J. Polym. Sci., Part B: Polym. Lett.* 1966, *4*, 317−322.
(31) Peters, R. A. Interfacial Tension and Hydrogen-Ion
Concentration. *Proc. R. Soc. Edinburgh, Sect. B: Biol. Sci.* 1931, *109*, 88−90.
(32) Betts, J. J.; Pethica, B. A. The Ionization Characteristics of
Monolayers of Weak Acids and Bases. *Trans. Faraday Soc.* 1956, *52*, 1581.
(33) Forth, J.; French, D. J.; Gromov, A. V.; King, S.; Titmuss, S.; Lord, K. M.; Ridout, M. J.; Wilde, P. J.; Clegg, P. S. Temperature- and pH-Dependent Shattering: Insoluble Fatty Ammonium Phosphate Films at Water-Oil Interfaces. *Langmuir* 2015, *31*, 9312.

(34) Gu, C.; Botto, L. Direct Calculation of Anisotropic Surface Stresses during Deformation of a Particle-Covered Drop. *Soft Matter* 2016, *12*, 705−716.
(35) Danov, K. D.; Stanimirova, R. D.; Kralchevsky, P. A.; Marinova,
K. G.; Alexandrov, N. A.; Stoyanov, S. D.; Blijdenstein, T. B. J.; Pelan,
E. G. Capillary Meniscus Dynamometry - Method for Determining the Surface Tension of Drops and Bubbles with Isotropic and Anisotropic Surface Stress Distributions. *J. Colloid Interface Sci.* 2015, *440*, 168−178.
(36) Nagel, M.; Tervoort, T. A.; Vermant, J. From drop-shape analysis to stress-fitting elastometry. *Adv. Colloid Interface Sci.* 2017, *247*, 33−51.
(37) Liu, X.; Shi, S.; Li, Y.; Forth, J.; Wang, D.; Russell, T. P. Liquid
Tubule Formation and Stabilization Using Cellulose Nanocrystal Surfactants. *Angew. Chem.* 2017, *129*, 12768−12772.
(38) Chai, Y.; Lukito, A.; Jiang, Y.; Ashby, P. D.; Russell, T. P. Fine- Tuning Nanoparticle Packing at Water−Oil Interfaces Using Ionic Strength. *Nano Lett.* 2017, *17*, 6453.
(39) Du, K.; Glogowski, E.; Emrick, T.; Russell, T. P.; Dinsmore, A.
D. Adsorption Energy of Nano- and Microparticles at Liquid−Liquid Interfaces. *Langmuir* 2010, *26*, 12518−12522.
(40) Zhang, Y.; Wang, S.; Zhou, J.; Zhao, R.; Benz, G.; Tcheimou,
S.; Meredith, J. C.; Behrens, S. H. Interfacial Activity of Non- amphiphilic Particles in Fluid-Fluid Interfaces. *Langmuir* 2017, *33*, 4511−4519.
(41) Meng, X.; Liu, L.; Ouyang, S.; Xu, H.; Wang, D.; Zhao, N.; Ye,
J. Nanometals for Solar-to-Chemical Energy Conversion: From Semiconductor-Based Photocatalysis to Plasmon-Mediated Photo-catalysis and Photo-Thermocatalysis. *Adv. Mater.* 2016, *28*, 6781−
6803.
(42) Hua, X.; Bevan, M. A.; Frechette, J. Competitive Adsorption between Nanoparticles and Surface Active Ions for the Oil-Water Interface. *Langmuir* 2018, *34*, 4830−4842.
(43) Edwards, C. J. C.; Stepto, R. F. T.; Semlyen, J. A. Studies of
Cyclic and Linear Poly(Dimethyl Siloxanes):7. Diffusion Behaviour in a Poor Solvent. *Polymer* 1982, *23*, 865−868.
(44) Fainerman, V. B.; Makievski, A. V.; Miller, R. The Analysis of
Dynamic Surface Tension of Sodium Alkyl Sulphate Solutions, Based on Asymptotic Equations of Adsorption Kinetic Theory. *Colloids Surf., A* 1994, *87*, 61−75.
(45) Ward, A. F. H.; Tordai, L. Time-Dependence of Boundary
Tensions of Solutions I. The Role of Diffusion in Time-Effects. *J. Chem. Phys.* 1946, *14*, 453−461.
(46) Huang, C.; Cui, M.; Sun, Z.; Liu, F.; Helms, B. A.; Russell, T. P.
Self-Regulated Nanoparticle Assembly at Liquid/Liquid Interfaces: A Route to Adaptive Structuring of Liquids. *Langmuir* 2017, *33*, 7994−8001.
(47) Cerda, E.; Mahadevan, L. Geometry and Physics of Wrinkling.
Phys. Rev. Lett. 2003, *90*, 074302.
(48) Knoche, S.; Vella, D.; Aumaitre, E.; Degen, P.; Rehage, H.; Cicuta, P.; Kierfeld, J. Elastometry of Deflated Capsules: Elastic Moduli from Shape and Wrinkle Analysis. *Langmuir* 2013, *29*,
12463−12471.
(49) Clegg, P. S. Fluid-Bicontinuous Gels Stabilized by Interfacial Colloids: Low and High Molecular Weight Fluids. *J. Phys.: Condens. Matter* 2008, *20*, 113101.
(50) Cicuta, P.; Vella, D. Granular Character of Particle Rafts. *Phys. Rev. Lett.* 2009, *102*, 138302.
(51) Vella, D.; Aussillous, P.; Mahadevan, L. Elasticity of an Interfacial Particle Raft. *Europhys. Lett.* 2004, *68*, 212−218.
(52) Xie, G.; Forth, J.; Chai, Y.; Ashby, P. D.; Helms, B. A.; Russell,
T. P. Compartmentalized, All-Aqueous Flow-Through-Coordinated Reaction Systems. *Chem* 2019, *1−13*. doi: DOI: 10.1016/ j.chempr.2019.07.016
(53) Zang, D.; Langevin, D.; Binks, B. P.; Wei, B. Shearing Particle Monolayers: Strain-Rate Frequency Superposition. *Phys. Rev. E: Stat., Nonlinear, Soft Matter Phys.* 2010, *81*, 011604.
(54) You, S. S.; Rashkov, R.; Kanjanaboos, P.; Calderon, I.; Meron, M.; Jaeger, H. M.; Lin, B. Comparison of the Mechanical Properties of

Self-Assembled Langmuir Monolayers of Nanoparticles and Phos- pholipids. *Langmuir* 2013, *29*, 11751−11757.
(55) Griesemer, S. D.; You, S. S.; Kanjanaboos, P.; Calabro, M.; Jaeger, H. M.; Rice, S. A.; Lin, B. The Role of Ligands in the Mechanical Properties of Langmuir Nanoparticle Films. *Soft Matter* 2017, *13*, 3125−3133.
(56) Garbin, V.; Jenkins, I.; Sinno, T.; Crocker, J. C.; Stebe, K. J. Interactions and Stress Relaxation in Monolayers of Soft Nano- particles at Fluid-Fluid Interfaces. *Phys. Rev. Lett.* 2015, *114*, 108301.
(57) Huerre, A.; Cacho-Nerin, F.; Poulichet, V.; Udoh, C. E.; De Corato, M.; Garbin, V. Dynamic Organization of Ligand-Grafted Nanoparticles during Adsorption and Surface Compression at Fluid-Fluid Interfaces. *Langmuir* 2018, *34*, 1020−1028.
(58) Mueggenburg, K. E.; Lin, X.-M.; Goldsmith, R. H.; Jaeger, H. M. Elastic Membranes of Close-Packed Nanoparticle Arrays. *Nat. Mater.* 2007, *6*, 656−660.